ASTRONOMY & ASTROPHYSICS
SUPPLEMENT SERIES

Astron. Astrophys. Suppl. Ser. **125,** 543-549 (1997)

Effective collision strengths for electron-impact excitation of nitrogen-like Mg VI

C.A. Ramsbottom and K.L. Bell

Department of Applied Mathematics and Theoretical Physics, The Queens University of Belfast, Belfast BT7 1NN, UK

Received January 13; accepted January 19, 1997

Abstract. Effective collision strengths for electron-impact excitation of the N-sequence ion Mg VI are evaluated in the close-coupling approximation using the multichannel R-matrix method. Twelve LS target eigenstates are included in the expansion of the total wavefunction, consisting of the eight $n = 2$ states with configurations $2s^22p^3$, $2s2p^4$ and $2p^5$, and the four $n = 3$ states with configuration $2s^22p^23s$. These 12 ionic states correspond to 23 fine-structure levels, leading to a total of 253 independent transitions. The effective collision strengths for all possible forbidden, semi-forbidden and allowed transitions are obtained by averaging the electron collision strengths, for a wide range of incident electron energies, over a Maxwellian distribution of velocities. Results are tabulated[1] for electron temperatures, T, in the range $\log T(\mathrm{K}) = 5.0$ to $\log T(\mathrm{K}) = 6.1$, which are the temperatures of interest for many astrophysical applications. We conclude that the effective collision strengths, for many of the forbidden lines considered, are significantly enhanced by autoionizing resonances converging to the target state thresholds in the collisional cross sections. The present calculations are the first to include such resonance phenomena.

Key words: atomic data — atomic processes

1. Introduction

The study of electron density and temperature diagnostics of solar plasmas using emission lines was first extensively reviewed by Gabriel & Jordan (1972), with more recent work including that of Feldman et al. (1992), Dwivedi (1994) and Mason & Monsignori Fossi (1994). A common procedure involves searching for intensity ratios which are sensitive to electron density (n_e) and/or electron temperature (T_e). In the present paper we consider the case of the Mg VI ion which has five fine-structure levels in the ground configuration, each of which is sensitive to electron density values relevant to the solar transition region. Therefore, although lines of Mg VI are relatively weak in the solar spectrum, some of the line ratios are potentially very useful for electron density/temperature diagnostics in different solar phenomena such as the quiet-Sun, active regions and solar flares (Bhatia & Mason 1980; Raju & Gupta 1993).

At present there is a paucity of atomic data available for the electron-impact excitation of the Mg VI ion. An early calculation by Saraph et al. (1969) produced LS collision strengths for transitions among the $2s^22p^3\ {}^4S^o$, ${}^2D^o$ and ${}^2P^o$ levels using the exact resonance distorted wave method. Only a limited number of incident electron energies were considered in this work which makes the Maxwellian averaging necessary to produce the astrophysically important effective collision strengths impossible. Davis et al. (1976) presented results for electron-impact excitation rate coefficients for a few selected transitions ($2s^22p^3\ {}^4S^o_{3/2} - 2s2p^4\ {}^4P^e_{1/2}$, $2s^22p^3\ {}^2P^o_{3/2} - 2s2p^4\ {}^2P^e_{3/2}$) in Mg VI. The calculations were carried out in the distorted wave approximation with exchange when required. Many of the rate coefficients produced by this work were expressed in terms of a simple two parameter fit. The most elaborate calculation to date was performed by Bhatia & Mason (1980), again utilizing the distorted wave method. They evaluated fine-structure collision strengths for transitions among the $2s^22p^3$ and $2s2p^4$ levels in Mg VI. The data, however, were presented for only three incident electron energies (10, 15, 20 Ryd.) and the effective collision strengths required for many astrophysical and plasma applications were not evaluated.

Clearly there is a need for a large and sophisticated close-coupling calculation to evaluate for the first time accurate effective collision strengths for the electron-impact excitation of Mg VI. The purpose of the present work is to perform the most elaborate evaluation to date which (a) includes a large number of target eigenstates in the

Send offprint requests to: C.A. Ramsbottom

[1] Table 5 is only available in electronic form at CDS via anonymous ftp to cdsarc.u-strasbg.fr (130.79.128.5) or via http://cdsweb.u-strasbg.fr/Abstract.html

Table 1. The orbital parameters (C, I, ξ) of the radial wavefunctions as indicated in Eq. (1)

Orbital	$C_{\rm jnl}$	$I_{\rm jnl}$	$\xi_{\rm jnl}$	Orbital	$C_{\rm jnl}$	$I_{\rm jnl}$	$\xi_{\rm jnl}$
1s	75.47140	1	11.69120	$\overline{4s}$	44.75401	1	3.14288
	4.96191	1	19.81840		−440.48331	2	3.19387
	0.10120	2	5.30819		1104.09003	3	3.19394
	13.81971	2	9.99860		−1038.47746	4	3.60095
	0.00039	2	4.07241				
				2p	25.22256	2	4.44405
2s	−21.53204	1	11.69120		21.80006	2	7.10836
	−0.71817	1	19.81840		10.49715	2	3.64321
	19.64494	2	5.30819		4.90313	2	14.97880
	−51.70492	2	9.99860				
	33.51006	2	4.07241	$\overline{3p}$	49.25869	2	2.52065
					−117.35998	3	3.18186
3s	9.86858	1	9.50846				
	−23.25848	2	3.67081	$\overline{3d}$	74.19637	3	4.38082
	10.98560	3	2.34889				

wavefunction representation of the Mg VI ion; (b) incorporates channel coupling and configuration-interaction effects by the inclusion of higher-lying levels; (c) produces collision strengths at a very fine mesh of incident electron energies to properly resolve the autoionizing resonances in the collision cross sections, which are known to significantly enhance the resulting effective collision strengths, and finally (d) to produce the astrophysically important fine-structure effective collision strengths over a wide range of electron temperatures.

2. The calculation

The R-matrix computer packages utilized in the present computations have been described in detail by Berrington et al. (1987). The twelve target eigenstates which are included in the wavefunction representation of the Mg VI parent ion are $2s^22p^3\ ^4S^o$, $^2D^o$, $^2P^o$; $2s2p^4\ ^4P^e$, $^2D^e$, $^2S^e$, $^2P^e$; $2p^5\ ^2P^o$; $2s^22p^23s\ ^4P^e$, $^2P^e$, $^2D^e$ and $^2S^e$. These target eigenstates are represented by configuration-interaction type wave-expansions constructed from seven orthogonal one-electron basis orbitals, consisting of four "spectroscopic" (1s, 2s, 2p, 3s) and three "pseudo" type orbitals ($\overline{3p}$, $\overline{3d}$, $\overline{4s}$), the latter being included to allow explicitly for additional correlation effects. The radial part of each of these orbitals may be expanded in the form:

$$P_{\rm nl}(r) = \sum_{\rm jnl} C_{\rm jnl} r^{I_{\rm jnl}} \exp(-\xi_{\rm jnl} r). \quad (1)$$

Since the R-matrix program requires all the target states to be represented in terms of a single-orbital basis, our choice of orbital parameters ($C_{\rm jnl}$, $I_{\rm jnl}$, $\xi_{\rm jnl}$) were as follows. The 1s, 2s and 2p orbital parameters were taken directly from the analysis of Clementi & Roetti (1974). The parameters for the 3s spectroscopic orbital were obtained by optimizing on the energy of the $2s^22p^23s\ ^2P^e$ state using the configuration-interaction computer package CIV3 as described by Hibbert (1975). The configurations $2s2p^4$, $2s^22p^23s$ and $2s2p^3[^3P]\overline{3p}$ were included in this optimization procedure. The parameters for the $\overline{3p}$ pseudo-orbital were similarly obtained by optimizing on the energy of the $2p^5\ ^2P^o$ state using the configurations $2s^22p^3$, $2p^5$ and $2p^4[^3P]\overline{3p}$, while those for the $\overline{3d}$ pseudo-orbital were found by optimizing on the $2s2p^4\ ^2P^e$ level with configurations $2s2p^4$, $2s^22p^2[^3P]\overline{3d}$ and $2s2p^3[^3P]\overline{3p}$. Finally the parameters for the only $n = 4$ pseudo-orbital, $\overline{4s}$, were obtained by optimizing on the energy of the $2s2p^4\ ^2D^e$ state with configurations $2s2p^4$, $2p^43s$, $2p^4\overline{4s}$ and $2s2p^3[^1D]\overline{3p}$. The parameters adopted for all seven orbitals are presented in Table 1. Table 2 displays the configurations, formed from this set of basis orbitals, which are retained in the wavefunction expansion for both even and odd parity target states.

The twelve target eigenstates included in the present calculation correspond to 23 fine-structure levels, each of which is assigned an index number in Table 3. Also shown in this table are the evaluated target state energies in atomic units relative to the $2s^22p^3\ ^4S^o$ ground state of Mg VI. An examination of these energies can give a reasonable measure of the accuracy of the ion representation utilized in the present calculation. On comparing with the most recent experimental values of Kaufman & Martin (1991) we see that most of the theoretical thresholds differ by less than 1% from the experimental values, the greatest disparity occuring for the $2s^22p^3\ ^4S^o - 2s^22p^3\ ^2D^o$ separation with a difference of less than 6%. Excellent agreement is also evident between the present thresholds and those

Table 2. Configurations included for even and odd parity target states. All configurations include $1s^2$

Odd Parity States	Even Parity States
$2s^22p^3$	$2s^22p^2$ [3s, $\overline{3d}$, $\overline{4s}$]
$2s^22p^2\overline{3p}$	$2s^22p3s\overline{3p}$
$2s^22p$ [$3s^2$, $\overline{3p}^2$, $\overline{3d}^2$, $\overline{4s}^2$]	$2s2p^4$
$2s2p^3$ [3s, $\overline{3d}$, $\overline{4s}$]	$2s2p^3\overline{3p}$
$2s^22p3s$ [$\overline{4s}$, $\overline{3d}$]	$2s2p^2$ [$3s^2$, $\overline{3p}^2$, $\overline{3d}^2$, $\overline{4s}^2$]
$2s2p^23s\overline{3p}$	$2s2p^23s$ [$\overline{3d}$, $\overline{4s}$]
$2s2p3s$ [$\overline{3p}^2$, $\overline{3d}^2$, $\overline{4s}^2$]	$2s2p3s^2\overline{3p}$
$2s2p3s^2$ [$\overline{3d}$, $\overline{4s}$]	$2s2p\overline{3p}\overline{3d}^2$
$2p^4\overline{3p}$	$2p^4$ [3s, $\overline{3d}$, $\overline{4s}$]
$2p^5$	$2p^33s\overline{3p}$
$2p^33s^2$	$2p^23s^2$ [$\overline{3d}$, $\overline{4s}$]
$2p^33s$ [$\overline{3d}$, $\overline{4s}$]	$2p^23s$ [$\overline{3p}^2$, $\overline{3d}^2$, $\overline{4s}^2$]
$2p^3$ [$\overline{3p}^2$, $\overline{3d}^2$, $\overline{4s}^2$]	
$2p^23s^2\overline{3p}$	
$2p3s^2$ [$\overline{3p}^2$, $\overline{3d}^2$, $\overline{4s}^2$]	

obtained by the International Opacity Project (Burke & Lennon, unpublished). Following the normal R-matrix procedures the present calculation has been carried out with the energies shifted to their experimental values. Also shown in Table 3 are the total number of configurations retained to describe each state.

A further indication of the reliability of the present wavefunction representation can be found by examining the close conformity between the length and velocity oscillator strength values for transitions between the target states. In Table 4 we present oscillator strengths, obtained using the configuration-interaction computer code CIV3 (Hibbert 1975), for optically allowed transitions among the lowest twelve LS states of Mg VI, in both the length and velocity formulations. Transitions for which the oscillator strength is less than 10^{-5} are not included. Excellent agreement is evident between the present length and velocity values with differences better than 9%. There is at present a severe lack of other available oscillator strengths for Mg VI. Hence, our comparison is limited to those obtained by the Opacity Project. Good agreement is, however, evident between their length values and the length values obtained by the present calculation. This would suggest that the present length values can be assigned an accuracy by using the difference between the present results and those from the Opacity Project. With a few exceptions, this would suggest an accuracy of better than 5%. We note that the results of Bhatia & Mason (1980) for the $2s^22p^3 - 2s2p^4$ transitions are always larger than both the present data and the Opacity Project values by typically 30%.

The theory describing the expansion of the Mg VI ion plus electron system has been discussed in detail by Burke & Robb (1975). The R-matrix boundary was set at 5.6 a.u., twenty continuum orbitals were included for each channel angular momentum and the electron-impact energy range of interest lies between 0 and 50 Rydbergs. All incident partial waves with total angular momentum $L \leq 12$, for both even and odd parities, and singlet, triplet and quintet multiplicities, were included in the wavefunction expansion. These seventy-eight partial waves were found to be sufficient to ensure convergence of the collision strengths for the optically forbidden transitions. Contributions from the partial waves with total angular momentum $L > 12$ become much more important for the dipole allowed transitions and need to be taken into account. It has been conclusively shown by Ramsbottom et al. (1994, 1995, 1996a, 1997), when investigating electron-impact excitation of N IV, Ne VII, S II and Ar IV respectively, that it is possible to estimate quite accurately these additional contributions for allowed transitions by assuming the partial collision strengths form a geometric series with a geometric scaling factor equal to the ratio of two adjacent terms. Contributions from the high partial waves $L > 12$ can be as much as $15-20\%$ for some of the slowest converging transitions.

The R-matrix computer packages produce collision strengths for transitions between LS states only. However, for many astrophysical and plasma applications it is often the collision strengths among the fine-structure levels which are required. Transforming to a jj-coupling scheme can easily be achieved by utilizing the program developed by Saraph (1978). Finally a thermally averaged effective collision strength ($\Upsilon_{\rm if}$) may be derived from the collision strength ($\Omega_{\rm if}$) by

$$\Upsilon_{\rm if}(T_{\rm e}) = \int_0^\infty \Omega_{\rm if}(E_{\rm f}) \exp(-E_{\rm f}/kT_{\rm e}) {\rm d}(E_{\rm f}/kT_{\rm e}) \qquad (2)$$

where $T_{\rm e}$ is the electron temperature in K, $E_{\rm f}$ the energy of the final electron and k is Boltzmann's constant.

3. Results and discussion

To properly resolve the complex autoionizing resonances in the collision cross sections for each transition, we have utilized a very fine mesh of incident impact energies ($\leq$0.0002 Ryd in the vicinity of the threshold regions). The detailed resonances located below the highest-lying target state threshold included in the present calculation ($2s^22p^23s\ ^2S^e$) are true structures, whereas those found at energies above this level (8.96 Ryd) are pseudo-resonances arising due to our inclusion of pseudo-orbitals in the wavefunction representation (Burke et al. 1981). For increasing temperatures this high impact energy region becomes much more important, hence it is necessary to average over the pseudo-resonances to prevent distortion of the results when the thermal averaging is performed.

Table 3. Target state energies (in a.u.) relative to the $2s^2 2p^3\ ^4S^o$ ground state of Mg VI. (a) Experimental Energies of Kaufman & Martin (1991), (b) Opacity Values (*unpublished*), (c) Bhatia & Mason (1980)

Index	J Level	Mg VI State	Present LS Energy	Expt.[a]	Opacity Project[b]	BAM[c]	No. Configs.
1	3/2	$2s^2 2p^3\ ^4S^o$	0.0000	0.0000	0.0000	0.0000	31
2	3/2	$2s^2 2p^3\ ^2D^o$	0.2668	0.2523	0.2592	0.2652	70
3	5/2						
4	1/2	$2s^2 2p^3\ ^2P^o$	0.3971	0.3827	0.3915	0.3762	86
5	3/2						
6	1/2	$2s2p^4\ ^4P^e$	1.1259	1.1341	1.1219	1.1283	70
7	3/2						
8	5/2						
9	3/2	$2s2p^4\ ^2D^e$	1.5657	1.5572	1.5560	1.6029	97
10	5/2						
11	1/2	$2s2p^4\ ^2S^e$	1.8455	1.8308	1.8372	1.8680	47
12	1/2	$2s2p^4\ ^2P^e$	1.9601	1.9403	1.9495	2.0214	85
13	3/2						
14	1/2	$2p^5\ ^2P^o$	2.9704	2.9741	2.9650		86
15	3/2						
16	1/2	$2s^2 2p^2 3s\ ^4P^e$	4.0865	4.0802	4.0985		70
17	3/2						
18	5/2						
19	1/2	$2s^2 2p^2 3s\ ^2P^e$	4.1527	4.1448	4.1648		85
20	3/2						
21	3/2	$2s^2 2p^2 3s\ ^2D^e$	4.2984	4.2776	4.3031		97
22	5/2						
23	1/2	$2s^2 2p^2 3s\ ^2S^e$	4.5254	4.4808	4.5164		47

Table 4. Oscillator strengths for optically allowed LS transitions in Mg VI (+) Bhatia & Mason (1980)

Transition	*Present*		*Opacity*		*BAM*[+]
$-f_L$	f_V	f_L	f_V		
$2s^2 2p^3\ ^4S^o - 2s2p^4\ ^4P^e$	0.1967	0.2158	0.2008	0.2168	0.261
$2s^2 2p^3\ ^4S^o - 2s^2 2p^2 3s\ ^4P^e$	0.0985	0.0996	0.1255	0.1285	
$2s^2 2p^3\ ^2D^o - 2s2p^4\ ^2D^e$	0.1168	0.1264	0.1180	0.1280	0.155
$2s^2 2p^3\ ^2D^o - 2s2p^4\ ^2P^e$	0.1679	0.1802	0.1680	0.1840	0.202
$2s^2 2p^3\ ^2D^o - 2s^2 2p^2 3s\ ^2P^e$	0.0442	0.0458	0.0465	0.0466	
$2s^2 2p^3\ ^2D^o - 2s^2 2p^2 3s\ ^2D^e$	0.0481	0.0490	0.0582	0.0591	
$2s^2 2p^3\ ^2P^o - 2s2p^4\ ^2D^e$	0.0348	0.0368	0.0347	0.0375	0.046
$2s^2 2p^3\ ^2P^o - 2s2p^4\ ^2S^e$	0.0708	0.0777	0.0718	0.0775	0.092
$2s^2 2p^3\ ^2P^o - 2s2p^4\ ^2P^e$	0.0913	0.0987	0.0893	0.0975	0.113
$2s^2 2p^3\ ^2P^o - 2s^2 2p^2 3s\ ^2P^e$	0.0705	0.0741	0.0635	0.0655	
$2s^2 2p^3\ ^2P^o - 2s^2 2p^2 3s\ ^2D^e$	0.0371	0.0382	0.0365	0.0378	
$2s^2 2p^3\ ^2P^o - 2s^2 2p^2 3s\ ^2S^e$	0.0168	0.0169	0.0248	0.0247	
$2s2p^4\ ^2D^e - 2p^5\ ^2P^o$	0.1012	0.1073	0.1020	0.1120	
$2s2p^4\ ^2S^e - 2p^5\ ^2P^o$	0.0380	0.0419	0.0373	0.0415	
$2s2p^4\ ^2P^e - 2p^5\ ^2P^o$	0.2025	0.2181	0.2067	0.2250	

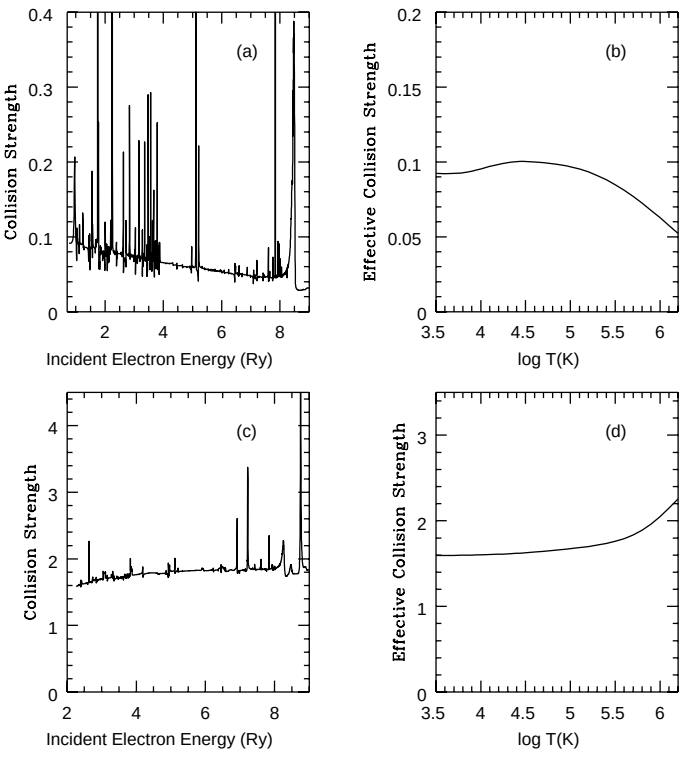

Fig. 1. Collision strength as a function of incident electron energy in Rydbergs, and the effective collision strength as a function of log temperature in Kelvin, for the $2s^22p^3\ {}^4S^o_{3/2} - 2s^22p^3\ {}^2P^o_{1/2}$ **a) and b)** and $2s^22p^3\ {}^4S^o_{3/2} - 2s2p^4\ {}^4P^e_{5/2}$ **c) and d)** fine-structure transitions

In Table 5 the effective collision strengths for all 253 possible independent transitions in Mg VI are presented for a wide range of electron temperatures ($\log T(\mathrm{K}) = 5.0 - \log T(\mathrm{K}) = 6.1$). The index values assigned to the fine-structure levels in Table 3 are utilized again here to denote a particular transition. It is very difficult to gauge the behavior of the effective collision strengths from such a large table. Hence, in order to illustrate the physical effects more clearly, we have chosen four particular transitions all involving the $2s^22p^3$ ground state configuration of Mg VI.

- $2s^22p^3\ {}^4S^o_{3/2} - 2s^22p^3\ {}^2P^o_{1/2}$ (Figs. 1a and b): an example of a spin forbidden transition from the ground state where the low-energy collision strength is strongly enhanced by resonances.
- $2s^22p^3\ {}^4S^o_{3/2} - 2s2p^4\ {}^4P^e_{5/2}$ (Figs. 1c and d): an example of an allowed transition from the ground state where contributions from the higher-partial waves $L > 12$ become more important as the temperature increases.
- $2s^22p^3\ {}^2D^o_{3/2} - 2s2p^4\ {}^2D^e_{5/2}$ (Figs. 2a and b): an example of an allowed transition out of a metastable state where the collision strength in the low-energy region is sensitive to configuration-interaction, channel coupling and resonance effects.
- $2s^22p^3\ {}^2P^o_{1/2} - 2p^5\ {}^2P^o_{1/2}$ (Figs. 2c and d): an example of a forbidden transition where resonance effects in the collision cross section do not significantly effect the corresponding effective collision strength.

In Figs. 1 and 2 we plot the collision strength as a function of incident electron energy in Rydbergs, and the corresponding effective collision strength as a function of log temperature in Kelvin, for each of the four transitions considered. Figures 1a and b show the results obtained for the $2s^22p^3\ {}^4S^o_{3/2} - 2s^22p^3\ {}^2P^o_{1/2}$ fine-structure forbidden transition. The low-energy collision strength is dominated by a mass of resonance structure which results in a slightly enhanced effective collision strength in the low temperature region. Such enhancements due to resonances converging to the target state thresholds is a common characteristic for forbidden transitions and has been consistently found by Ramsbottom et al. (1994, 1995, 1996a, 1997) when investigating electron-impact excitation of N IV, Ne VII, S II and Ar IV respectively. It is difficult to gauge by how much the resonances have enhanced the effective collision strength due to the lack of other theoretical data available for comparison. Also common for forbidden transitions of this kind is the decrease in the effective collision strength as the temperature increases.

In Figs. 1c and d we present the collision strength and the corresponding effective collision strength for the dipole-allowed $2s^22p^3\ {}^4S^o_{3/2} - 2s2p^4\ {}^4P^e_{5/2}$ fine-structure transition. The most noticeable feature is the absence of resonance structure in the collision cross section across the entire range of electron-impact energies. This leads to an almost constant effective collision strength in the low temperature region. Contributions from the high-partial waves $L > 12$, however, become more and more important as the temperature increases, resulting in a larger effective collision strength at the high temperatures. This behavior is common for dipole-allowed transitions of this kind. In contrast the collision strength plotted in Fig. 2a for the allowed $2s^22p^3\ {}^2D^o_{3/2} - 2s2p^4\ {}^2D^e_{5/2}$ fine-structure transition has an abundance of resonance structure in the low-energy region superimposed on an almost constant background cross section. The corresponding effective collision strength for this transition, plotted in Fig. 2b, is as expected significantly enhanced in the low temperature region by the presence of these autoionizing resonances converging to the target state thresholds. The characteristic rise of the effective collision strength for this allowed transition is again evident in the high temperature region.

Finally in Figs. 2c and d we present the results for the remaining forbidden transition considered, the $2s^22p^3\ {}^2P^o_{1/2} - 2p^5\ {}^2P^o_{1/2}$. The absence of autoionizing resonances in the collision strength and the almost constant background cross section leads to a uniform effective collision strength across the entire temperature range considered. At the higher temperatures, however, the effective collision strength does seem to be

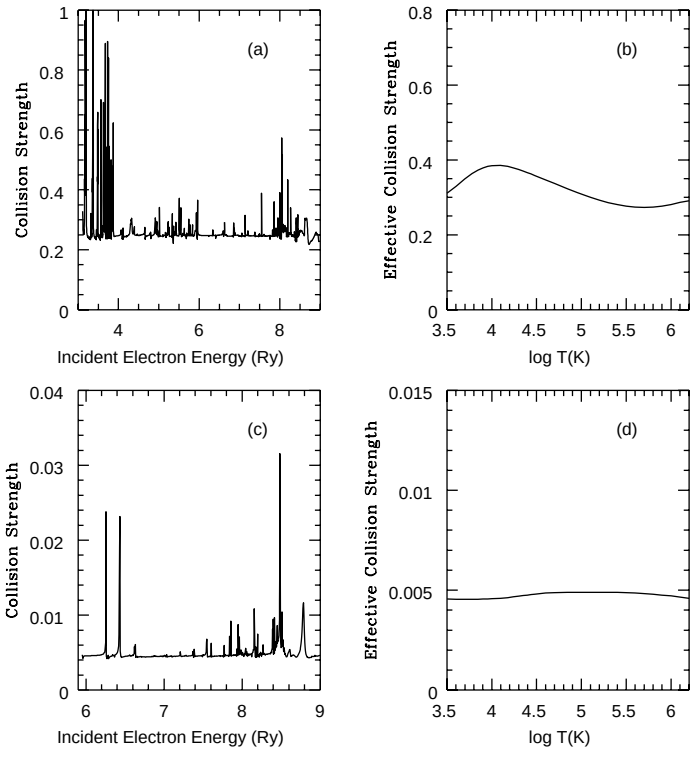

Fig. 2. Collision strength as a function of incident electron energy in Rydbergs, and the effective collision strength as a function of log temperature in Kelvin, for the $2s^2 2p^3\ ^2D^o_{3/2} - 2s2p^4\ ^2D^e_{5/2}$ **a) and b)** and $2s^2 2p^3\ ^2P^o_{1/2} - 2p^5\ ^2P^o_{1/2}$ **c) and d)** fine-structure transitions

decreasing which is characteristic for a forbidden transition. Evidently there is a need for a further sophisticated theoretical calculation to verify the results presented here in the absence of a meaningful comparison.

The Mg VI emission lines in the solar spectrum should be routinely detected by both the Coronal Diagnostic Spectrometer (CDS) and Solar Ultraviolet Measurements of Emitted Radiation (SUMER) instruments on the Solar and Heliosphere Observatory, which cover the wavelength regions 150 – 800 Å and 500 – 1600 Å, respectively (Harrison et al. 1995; Wilhelm et al. 1995). In the near future we therefore intend to compare CDS/SUMER observations with Mg VI theoretical line strengths generated using our atomic data, to investigate the usefulness of the lines as diagnostics.

4. Conclusions

The multichannel R-matrix method has been used extensively in the past by Ramsbottom et al. (1994, 1995, 1996a, 1997) to produce effective collision strength for electron-impact excitation of astrophysically important N IV, Ne VII, S II and Ar IV. These calculations have been proved to have a typical accuracy of 10% or better (Keenan et al. 1995, 1996). We would expect the present effective collision strengths to have a similar accuracy, but it is difficult to assess due to the lack of theoretical data available for comparison, and because the astrophysical diagnostic applications have not yet been performed using this new atomic data. In the near future theoretical line intensities, calculated using the present results, will be compared with high resolution optical observations of planetaries, and this will assist in predicting the accuracy more precisely. The most serious error in the tabulated data occurs due to the omission of higher-lying target states in the wavefunction representation of the Mg VI ion. To quantify these errors, a much more sophisticated calculation would need to be performed. The present work is the most elaborate to date due to the fact that extensive configuration-interaction wavefunctions were utilized, and a very fine mesh of electron-impact energies was used to properly delineate the detailed resonance structures in the collisional cross sections. The neglect of these autoionizing resonances would have a dramatic effect on the resulting effective collision strengths. In addition the present calculation took care to include correlation terms in the total wavefunction to compensate for the omitted higher-lying levels.

Acknowledgements. The work reported in this paper has been supported by PPARC, under the auspices of a Rolling Grant GR/L 20276, and the computations were carried out on the CRAY J932-SN9522 at Rutherford Appleton Laboratory. We are grateful to Prof. F.P. Keenan for helpful discussions.

References

Berrington K.A., Burke P.G., Butler K., Seaton M.J., Storey P.J., Taylor K.T., Yu Yan, 1987, J. Phys. B: At. Mol. Phys. 20, 6379

Bhatia A.K., Mason H.E., 1980, MNRAS 190, 925

Burke P.G., Robb W.D., 1975, Advances in Atomic and Molecular Physics. In: Bates D.R. and Bederson B. (eds.). Academic Press, New York Vol. II, p. 143

Burke P.G., Sukumar C.V., Berrington K.A., 1981, J. Phys. B: At. Mol. Phys. 14, 289

Clementi E., Roetti C., 1974, At. Data Nucl. Data Tab. 14, 177

Davis J., Kepple P.C., Blaha M., 1976, J. Quant. Spectr. Rad. Trans. 16, 1043

Dwivedi B.N., 1994, Adv. Space Sci. Rev. 65, 289

Feldman U., Mandelboum P., Seely J.F., Doschelc G.A., Gursley H., 1992, ApJS 81, 387

Gabriel A.H., Jordan C., 1972, Case Studies in Atomic Collison Physics. In: McDaniel E. and McDowel M.C. (eds.), Vol. II. North-Holland Publ.Co., Amsterdam, p. 210

Harrison R.A., et al., 1995, Solar Phys. 162, 233

Hibbert A., 1975, Comput. Phys. Commun. 9, 141

Kaufman V., Martin W.C., 1991, J. Phys. Chem. Ref. Data. 20, 83

Keenan F.P., Ramsbottom C.A., Bell K.L., Berrington K.A., Hibbert A., Feibelman W.A., Blair W.P., 1995 ApJ 438, 500

Keenan F.P., Aller L.H., Bell K.L., Hyung S., McKenna F.C., Ramsbottom C.A., 1996, MNRAS 281, 1073
Mason H.E., Monsignori Fossi B.C., 1994, A&AR 6, 123
Raju P.K., Gupta A.K., 1993, Solar Phys. 145, 241
Ramsbottom C.A., Berrington K.A., Hibbert A., Bell K.L., 1994, Phys. Scr. 50, 246
Ramsbottom C.A., Berrington K.A., Bell K.L., 1995, At. Data Nucl. Data Tab. 61, 105
Ramsbottom C.A., Bell K.L., Stafford R.P., 1996a, At. Data Nucl. Data Tab. 63, 57
Ramsbottom C.A., Bell K.L., 1997, At. Data Nucl. Data Tab. 66, 65 (now published)
Saraph H.E., 1978, Comput. Phys. Commun. 15, 247
Saraph H.E., Seaton M.J., Shemming J., 1969, Phil. Trans. Roy. Soc. London 264, 77
Wilhelm K., et al., 1995, Solar Phys. 162, 189